Pulsed Interaction Signals as a Route to Biological Pattern Formation

Eduardo H. Colombo,[1,2,3,*] Cristóbal López,[3,†] and Emilio Hernández-García[3,‡]
[1]Department of Ecology and Evolutionary Biology, Princeton University, Princeton, New Jersey 08544, USA
[2]Department of Ecology, Evolution, and Natural Resources, Rutgers University, New Brunswick, New Jersey 08901, USA
[3]Instituto de Física Interdisciplinar y Sistemas Complejos (IFISC), CSIC-UIB,
Campus Universitat Illes Balears, 07122 Palma de Mallorca, Spain

(Received 13 July 2022; accepted 4 January 2023; published 3 February 2023; corrected 14 September 2023)

We identify a mechanism for biological spatial pattern formation arising when the signals that mediate interactions between individuals in a population have pulsed character. Our general population-signal framework shows that while for a slow signal-dynamics limit no pattern formation is observed for any values of the model parameters, for a fast limit, on the contrary, pattern formation can occur. Furthermore, at these limits, our framework reduces, respectively, to reaction-diffusion and spatially nonlocal models, thus bridging these approaches.

DOI: 10.1103/PhysRevLett.130.058401

Introduction.—One of the striking manifestations of self-organization in complex systems is the emergence of regular spatial patterns at scales much larger than the ones associated with the individual components [1]. In biological populations this phenomenon has been observed in many contexts including semi-arid vegetation [2–4], bird swarms [5,6], or bacteria colonies [7,8]. Besides being fascinating, pattern formation has been shown to critically affect the stability and resilience of ecosystems [9,10].

Behind the mechanisms responsible for self-organization there is often an agent or substance working as a signal that mediates the interactions. Signals have distinct emission protocols, propagation dynamics, and occur in a wide range of temporal and spatial scales [11]. For example, species might use acoustic [12], visual [13], or chemical [14] signals to attract, repel, harm, or support targeted individuals. It is this exchange of signals and the details of its dynamics that ultimately drive self-organization process [15,16] and, consequently, control other key macroscopic outcomes [9,17].

Despite the numerous studies analyzing how interactions control pattern formation, the focus has been mostly on continuous and smooth signal dynamics. This overlooks interactions that are mediated by flashing pulsed signals. Therefore, how this fine-scale dynamics scales-up affecting pattern formation is poorly understood. Here we show that a timescale transition from slow (smooth) to fast (pulsed) signal dynamics creates a route to pattern formation alternative to the most studied ones arising from Turing-like mechanisms [18].

This finding is obtained by studying a general activator-inhibitor (population-signal) model, where a population interacts through the release of harmful signals. Our study extends standard activator-inhibitor structure [19,20], by explicitly describing the fine-scale dynamics associated with the release and spreading of signals. This framework recovers two distinct structures at the regimes of slow and fast signal dynamics that can lead to qualitative changes in spatial stability. For slow signal (with timescales similar to those of the population), we recover a standard reaction-diffusion system which, for a broad set of population and signal dynamics, does not exhibit Turing instability for any values of model parameters. For the same system dynamics, but with sufficiently fast signals, the system can be described by a single integrodifferential equation, where the toxic effects are captured by a competitive nonlocal spatial interaction. In this limit, spatial instability can occur leading to pattern formation.

Since we explicitly derive the underlying interference competition mechanism behind the nonlocal effective description, these results address a long-standing shortcoming: that paradigmatic nonlocal models of competitive type leading to spatial patterns have been usually proposed phenomenologically with no systematic derivation [4,21,22]. In the cases in which such derivation has been provided, the resulting equation did not have the characteristics needed for pattern-forming instabilities (see, for example, Ref. [23]).

Model.—Our aim is to model an ensemble of simple organisms in a one-dimensional spatial domain (we do not expect this dimensional restriction to be essential for our results). They move, reproduce, and release harmful signals in the form of pulses. These pulses can have biochemical origins, such as a toxic substance, but can also be physical, in the form of electricity, heat, sound, and light, which can compromise the targets' survival, and lead to a competing dynamics among the individuals [13,24,25]. We describe this scenario at the population level by the following general density-field description,

$$\tau_\rho \partial_t \rho = \mathcal{L}(\rho, \partial_x \rho) - \epsilon \rho \phi, \tag{1}$$

$$\tau_\phi \partial_t \phi = L(\phi, \partial_x \phi) + \mathcal{R}_\rho(x,t), \tag{2}$$

where ρ and ϕ are the population density and signal intensity, respectively. $\mathcal{L}$ and L give the population and signal dynamics when uncoupled, including diffusion or other transport processes; τ_ρ and τ_ϕ explicitly set the timescales for the population and signal dynamics, respectively; and ϵ is an exposition factor related to the population sensitivity to the toxin, which is released according to $\mathcal{R}_\rho$.

We consider that signal releases occur in pulses that are controlled by the population density in the following manner: Their starting time-space locations $\{t_i, x_i\}$ are independent Poisson random events with a probability of occurring within small intervals dx and dt given by $\alpha\rho(x,t)dxdt$. The pulses have duration $\bar{\delta}$, negligible spatial extent, and equal intensities I_0:

$$\mathcal{R}_\rho(x,t) = \sum_i I_0 \Pi_{\bar{\delta}}(t - t_i)\delta(x - x_i), \tag{3}$$

where $\Pi_{\bar{\delta}}(t)$ is the indicator function of the time interval $[0, \bar{\delta}]$. The expected interevent time, $\langle t_{i+1} - t_i \rangle$, is given by $\tau_R = 1/(N(t)\alpha)$, where $N(t) = \int_{-\infty}^{+\infty} \rho(x)dx$ is the total population size. Equations (1)–(3) together establish the model studied in this Letter, being constituted by a continuous population model but with a pulsed spatiotemporal dynamics for the signal [26].

The characteristic timescales are, besides τ_ρ and τ_ϕ, the duration of the pulses, $\bar{\delta}$, and the mean pulse interevent time, τ_R. We will focus on cases in which pulse duration is much shorter than release interevent time, which is itself much shorter than population dispersal and other demographic processes, $\bar{\delta} \ll \tau_R \ll \tau_\rho$. This means that there is a timescale separation between interaction events and their consequences to population dynamics.

In the following, we investigate how the system spatial stability changes as a function of the signal timescale, τ_ϕ. We obtain effective descriptions for the population-toxin dynamics and the respective pattern forming conditions for (a) the *slow signal-dynamics limit*, in which the toxin-field relaxation is slow, being comparable to population dynamics timescales $\tau_\phi/\tau_\rho \sim 1$, and thus $\bar{\delta}, \tau_R \ll \tau_\phi$; and (b) *fast signal-dynamics limit*, when signal response is the faster of all the timescales, $\tau_\phi \ll \bar{\delta}, \tau_R, \tau_\rho$ (see Fig. 1).

Slow signal-dynamics limit.—When $\tau_\phi/\tau_\rho \sim 1$ the interevent release time is much shorter than population and signal timescales, $\tau_R \ll \tau_\phi, \tau_\rho$. Then, the toxin field ϕ in Eq. (2) feels the average of the toxin release pulses, which are many and occur too fast for ϕ to follow them. Consequently, we can replace $\mathcal{R}_\rho$ by its average over small time windows $\Delta t \ll \tau_\phi$ and small vicinities Δx:

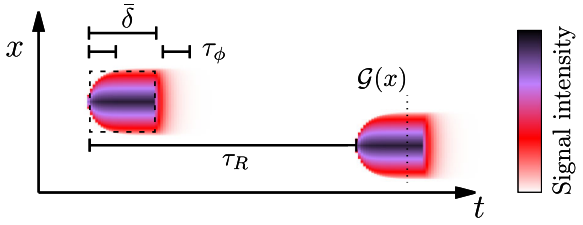

FIG. 1. Schematic representation of the timescales of the signal $\phi(x,t)$ in the fast signal-dynamics limit ($\tau_\phi \to 0$). Signal response to two signal release pulses is shown for moderately fast signals. ϕ remains mainly localized in time within the pulse duration $\bar{\delta}$ (dashed rectangle). The rising and decaying parts of the signal are indicated by the two short segments close to the label τ_ϕ. The vertical dotted line indicates an intermediate time at which signal intensity attains the steady $\mathcal{G}$ profile. In the plot, the lapse between pulses is set to τ_R (the mean interevent time) and the field ϕ spreads according to Eq. (7) [with $\nu = 4$ and $\mu = 1$ as in Fig. 3(b)].

$$\langle \mathcal{R}_\rho(x,t) \rangle \equiv \frac{1}{\Delta t \Delta x} \int_{-\Delta t}^{0} \int_{-\frac{\Delta x}{2}}^{\frac{\Delta x}{2}} \mathcal{R}_\rho(x + x', t + t')dx'dt'. \tag{4}$$

Using Eq. (3), $\langle \mathcal{R}_\rho(x,t) \rangle = (\Delta x \Delta t)^{-1} \sum_{i=1}^{n_R} I_0 \bar{\delta} = I_0 \bar{\delta} n_R/(\Delta x \Delta t)$, where n_R is the number of pulses that have occurred during the considered space-time window. Noting that pulses are independent events, n_R for each cell follows a Poisson distribution with mean $\alpha\rho(x,t)\Delta x \Delta t$. If Δt is chosen sufficiently large (but still much smaller than τ_ϕ) n_R becomes large and its coefficient of variation (ratio of standard deviation to mean) vanishes so that fluctuations can be neglected. Thus $n_R \approx \alpha\rho(x,t)\Delta x \Delta t$. As a consequence, in the slow signal limit, $\langle \mathcal{R}_\rho(x,t) \rangle \approx I_0 \bar{\delta} \alpha \rho(x,t)$. The other terms in Eqs. (1)–(2) can also be coarse-grained but, due to their slow response times, they remain constant and unaffected by the procedure: $\langle \rho \rangle \simeq \rho$, $\langle \phi \rangle \simeq \phi$, $\langle \phi\rho \rangle \simeq \phi\rho$.

Fast signal-dynamics limit.—In this fast limit, $\tau_\phi/\tau_\rho \to 0$, the signal dynamics is much faster than any other process. Then, we can expect the signal field to be always in constant equilibrium with the release events: it immediately reaches a fixed stationary profile, $\mathcal{G}(x)$ during the pulse duration, $0 < t - t_i < \bar{\delta}$, and dissipates immediately when release ceases (we assume a L dynamics that leads to signal dissipation in the absence of releases). In Fig. 1, we present a schematic representation of the fast signal propagation, highlighting with a dashed rectangle the area in which signals would be confined taking $\tau_\phi \to 0$. The profile $\mathcal{G}$ at intermediate times (such as the vertical dotted line in Fig. 1) can be obtained by solving Eq. (2) under the limit $\tau_\phi \to 0$. For a single pulse in (3) at $x = 0$, $L(\mathcal{G}, \partial_x \mathcal{G}) + I_0 \delta(x) = 0$. The conditions $\tau_\phi \ll \bar{\delta} \ll \tau_R$ guarantee that pulses are nonoverlapping, so that the solution of Eq. (2) can be built just adding up the successive responses to the different pulses: $\phi(x,t) \approx \sum_i \mathcal{G}(x - x_i)\Pi_{\bar{\delta}}(t - t_i)$. We now perform, as in

Eq. (4), an average of Eq. (1) over small intervals Δx and $\Delta t \ll \tau_\rho$. Because of timescale separation, all terms remain unaltered except the last one containing ϕ, which becomes $\langle \rho\phi \rangle \approx \rho\langle\phi\rangle$. Calculation of this last average is performed in detail in the Supplemental Material [27], with the final result $\langle\phi\rangle \approx \bar{\delta}\alpha[\mathcal{G} * \rho]$, where $\mathcal{G} * \rho \equiv \int \mathcal{G}(x - x')\rho(x', t)dx'$.

In summary, from model (1)–(3), the slow signal-dynamics limit ($\bar{\delta} \ll \tau_R \ll \tau_\phi, \tau_\rho$) leads to

$$\tau_\rho \partial_t \rho = \mathcal{L}(\rho, \partial_x \rho) - \epsilon\rho\phi,$$
$$\tau_\phi \partial_t \phi = L(\phi, \partial_x \phi) + \bar{R}\rho, \quad \text{with} \quad \bar{R} \equiv \alpha\bar{\delta}I_0. \tag{5}$$

Fast signal dynamics ($\tau_\phi \ll \bar{\delta} \ll \tau_R \ll \tau_\rho$) gives

$$\tau_\rho \partial_t \rho = \mathcal{L}(\rho, \partial_x \rho) - \bar{\epsilon}\rho[\mathcal{G} * \rho], \quad \text{with} \quad \bar{\epsilon} \equiv \epsilon\bar{\delta}\alpha. \tag{6}$$

Regardless of the choice of $\mathcal{L}(\rho, \partial_x\rho)$ and $L(\phi, \partial_x\phi)$, the fact that the two regimes lead to different coarse-grained models suggests that their spatial stability also differs. In fact, it can be shown that pattern formation does not occur in the slow signal limit [Eq. (5)] for a large class of operators (see Ref. [27] for precise conditions on $\mathcal{L}$ and L). However, for this same class in the fast limit, it is well known that Eq. (6) can lead to spatial patterns when the signal profile $\mathcal{G}$ is sufficiently platykurtic [32,33].

A particular example.—We illustrate the above developments with the following dynamics:

$$\mathcal{L}(\rho, \partial_x\rho) = (D_\rho \partial_{xx} + r)\rho,$$
$$L(\phi, \partial_x\phi) = D_\phi \partial_x(\phi^{\nu-1}\partial_x\phi) - [\gamma\phi^{\mu-1}]\phi, \tag{7}$$

which models populations of organisms moving Brownianly with diffusion coefficient D_ρ and reproducing with growth rate r. This choice is a fundamental building block for more complex population dynamics models [34]. For the signal dynamics, Eq. (7) gives a generalized nonlinear diffusion-decay process characterized by exponents $\nu, \mu > 0$. It allows us to consider the case where diffusion and decay are sensitive to signal intensity in a negative ($\nu, \mu < 1$) or positive ($\nu, \mu > 1$) manner, unraveling important channels through which environment structure (e.g., propagation in porous media, leading to $\nu > 1$, see Ref. [35]) and mediator interspecific biochemical interactions [24,34,36–40] can affect signal propagation dynamics.

Linear stability analysis and pattern formation.—The pattern-forming stability conditions of model (1)–(3) with the choice (7) can be obtained in the above studied timescale limits. For slow signal dynamics [Eq. (5)] the nontrivial homogeneous steady state is $\rho_0 = \gamma(r/\epsilon)^\mu/\bar{R}$, $\phi_0 = r/\epsilon$. Standard linear perturbation around this state identifies that all perturbation growth rates are negative for any value of parameters, implying the stability of the homogeneous state. Hence, no pattern-forming instability can arise.

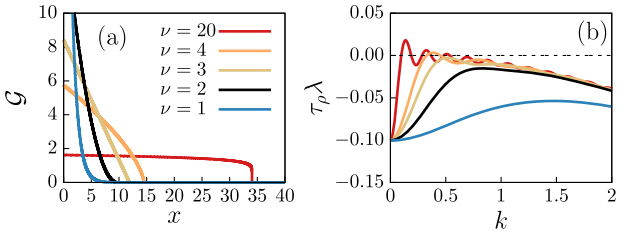

FIG. 2. (a) Profile $\mathcal{G}(x)$ from Eq. (8) and several ν. (b) Corresponding growth rates $\lambda(k)$ of perturbations to the homogeneous solution, as a function of perturbation wave number k. Parameters are $D_\rho = 0.01$, $\mu = 1$, $\bar{\epsilon} = r = 1$, $D_\phi = \gamma = 1$, and $I_0 = 10^2$.

For fast signal dynamics the model reduces to a single nonlocal equation, Eq. (6), with integral kernel $\mathcal{G}$. This is the solution of $L(\mathcal{G}, \partial_x\mathcal{G}) + I_0\delta(x) = 0$, an equation that can be solved exactly [28] for the particular choice (7) discussed here (additional details are in [27]) giving

$$\mathcal{G}(x) = A[1 - (1-q)|sx|]^{\frac{1}{1-q}}, \qquad A = \left[\frac{I_0}{2D_\phi}\sqrt{\frac{\mu+\nu}{2\kappa}}\right]^{\frac{2}{\mu+\nu}}, \tag{8}$$

with $q = 1 + (\mu - \nu)/2$, $s^2 = 2\kappa A^{\mu-\nu}/(\mu + \nu)$, and $\kappa = \gamma/D_\phi$. If $q < 1$ the support of this solution is restricted to $|x| \leq 1/(1-q)$.

Figure 2(a) presents the different shapes of $\mathcal{G}(x)$ as ν increases, while assuming linear decay ($\mu = 1$). The homogeneous steady solution is $\rho_0 = r/(\bar{\epsilon}\tilde{\mathcal{G}}(0))$, where $\tilde{\mathcal{G}}(k)$ is the Fourier transform of $\mathcal{G}$. Growth rates of periodic perturbations of wave number k to the homogeneous state are given by $\tau_\rho\lambda(k) = -D_\rho k^2 - r\tilde{\mathcal{G}}(k)/\tilde{\mathcal{G}}(0)$ and are shown in Fig. 2(b). Pattern formation requires that, for some k, $\tilde{\mathcal{G}}$ assumes a sufficiently negative value, yielding $\lambda(k) > 0$ [32]. For the present case, this occurs if toxin diffusion has a stronger sensitivity to concentration when compared to the decay process, $\nu > \mu + 2$. The marginal case, $\nu = \mu + 2$ ($\nu = 3$ with $\mu = 1$ in Fig. 2), corresponds to the triangular kernel and the limit case $\nu \to \infty$ to the (most used) top hat kernel, which is well known to lead to pattern formation [21,41–43]. Thus, in contrast to the slow signal-dynamics limit, pattern formation can occur under fast signal dynamics, showing the importance of pulsed dynamics on the macroscopic behavior of the system.

To support these analytical findings, we show in Fig. 3 direct numerical simulations (see Supplemental Material for the numerical integration scheme [27]) of Eqs. (1)–(3) and (7) (with $\mu = 1$, $\nu = 4$) for a slow (a) and a fast (b) signal-dynamics regimes. This is done by keeping the population timescale at $\tau_\rho = 1/r = 1$ for both plots, and selecting the signal timescale corresponding to $\tau_\phi = 1 \sim \tau_\rho$, and $\tau_\phi/\tau_\rho = 1/500 \ll 1$, respectively. In agreement with the analytical results, for the slow signal dynamics pattern formation does not occur for any of the parameter

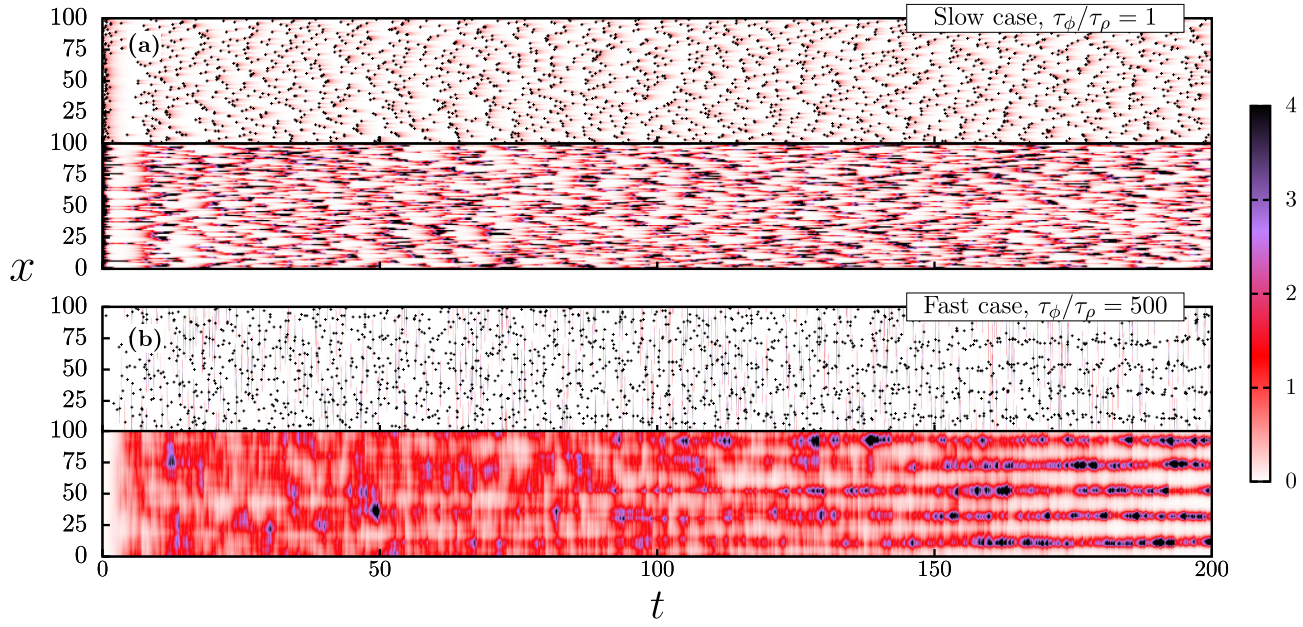

FIG. 3. Temporal evolution of signal and population fields for the slow (a) and fast (b) signal regimes. The system is a line of length 100 with periodic boundary conditions. Colors indicate field intensity $\phi(x,t)$ (upper panels), and population density relative to the (fast-signal limit) homogeneous state, $\rho(x,t)/\rho_0$ (bottom panels). In the upper panels crosses indicate release instants and positions (not all releases are captured by the finite resolution of the heat map). Data from numerical integration of Eqs. (1)–(3), using a Euler scheme with $\delta t = 10^{-6}$ and $\delta x = 1.0$. The dynamics is given by Eq. (7) with $D_\rho = 10^{-2}$, $r = \tau_\rho = 1$, $\alpha = 10^2$, $\bar{\delta} = 10^{-2}$, and $\epsilon = 10$. Signal dynamics is set by $\mu = 1$ and $\nu = 4$, scaled by τ_ϕ, in such a way that $D_\phi/4 = \gamma = 1/\tau_\phi$ and $I_0 = 10^2/\tau_\phi$. The slow and fast regimes were obtained setting $\tau_\phi = 1$ and $\tau_\phi = 1/500$, respectively. Mean interpulse interval is in both cases $\tau_R = 1/(N(t)\alpha) \simeq 10^{-1}$ (for a schematic closeup of the signal field in the fast-signal regime see Fig. 1).

values we have checked [Fig. 3(a)]. On the contrary, in the fast limit patterns develop, since $\nu > \mu + 2$. Spatial population periodicity is seen to emerge at long times in Fig. 3(b), and the spatial pattern remains stable afterwards (see Ref. [27]). The wavelength of the final pattern can be analytically estimated as $2\pi/k^\star \simeq 16.5$, where $k^\star$ is the fastest growing mode in Fig. 2(b). This is roughly close to the periodicity seen in Fig. 3(b) (see also Fig. S2 in Supplemental Material [27]).

Final remarks and discussion.—Our framework allowed us to see how different fine-scale signal dynamics impact at a coarser scale. It recovers standard reaction-diffusion [19,20] schemes in the slow-signal limit and integrodifferential schemes [32,44] in the fast-signal limit, working as a bridge between the two mostly used formalisms to describe interacting populations.

We crucially note that these two descriptions can lead to different macroscopic outcomes. In this Letter, we focused on showing that, for the same population and mediator dynamics, a transition from slow to fast pulsed signals can effectively lead to spatially extended interference competition in such a way that pattern formation occurs [21,23,32].

Our findings are of relevance in situations, from chemistry to ecology, in which interactions between the entities are mediated by pulses that are short and fast compared to reaction processes. More broadly, they stress crucial channels through which environment and individual-level behavior can control system spatial organization [45]. For example, our approach can be extended to cases in which signals regulate individual mobility [46,47], a mediation that has already shown to be relevant for population survival and spatial patterns [15,48]. Developmental programs can also explore these channels to engineer specific morphologies [26,49]. Further extension aiming at concrete problems should include realistic features such as state-dependent signal emissions [50,51] accounting for individuals response to attacks, memory [16], persistence [15], and multisignal mediation where signals establish a set of distinct biochemical interactions [11].

We acknowledge Ricardo Martinez-Garcia for a critical reading of the manuscript. This work has been supported by the Severo Ochoa and Maria de Maeztu Program for Centers and Units of Excellence in R&D, Grant No. MDM-2017-0711 funded by MCIN/AEI/10.13039/501100011033.

*ecolombo@princeton.edu
†clopez@ifisc.uib-csic.es
‡emilio@ifisc.uib-csic.es

[1] M. Rietkerk and J. Van de Koppel, Trends Ecol. Evol. **23**, 169 (2008).

[2] C. A. Klausmeier, Science **284**, 1826 (1999).
[3] J. von Hardenberg, E. Meron, M. Shachak, and Y. Zarmi, Phys. Rev. Lett. **87**, 198101 (2001).
[4] C. Fernandez-Oto, M. G. Clerc, D. Escaff, and M. Tlidi, Phys. Rev. Lett. **110**, 174101 (2013).
[5] T. Vicsek, A. Czirók, E. Ben-Jacob, I. Cohen, and O. Shochet, Phys. Rev. Lett. **75**, 1226 (1995).
[6] A. Attanasi, A. Cavagna, L. Del Castello, I. Giardina, T. S. Grigera, A. Jelić, S. Melillo, L. Parisi, O. Pohl, E. Shen *et al.*, Nat. Phys. **10**, 691 (2014).
[7] E. Ben-Jacob and P. Garik, Nature (London) **343**, 523 (1990).
[8] R. Tyson, S. Lubkin, and J. D. Murray, Proc. R. Soc. B **266**, 299 (1999).
[9] M. Rietkerk, S. C. Dekker, P. C. de Ruiter, and J. van de Koppel, Science **305**, 1926 (2004).
[10] J. A. Bonachela, R. M. Pringle, E. Sheffer, T. C. Coverdale, J. A. Guyton, K. K. Caylor, S. A. Levin, and C. E. Tarnita, Science **347**, 651 (2015).
[11] J. M. Smith, D. Harper *et al.*, *Animal Signals* (Oxford University Press, New York, 2003).
[12] R. Martínez-García, J. M. Calabrese, T. Mueller, K. A. Olson, and C. López, Phys. Rev. Lett. **110**, 248106 (2013).
[13] T. Caro and W. L. Allen, Phil. Trans. R. Soc. B **372**, 20160344 (2017).
[14] J. W. Larkin, X. Zhai, K. Kikuchi, S. E. Redford, A. Prindle, J. Liu, S. Greenfield, A. M. Walczak, J. Garcia-Ojalvo, A. Mugler *et al.*, Cell Syst. **7**, 137 (2018).
[15] L. Giuggioli, J. R. Potts, and S. Harris, PLoS Comput. Biol. **7**, e1002008 (2011).
[16] J. R. Potts and M. A. Lewis, J. R. Soc. Interface **13**, 20160059 (2016).
[17] L. Niehaus, I. Boland, M. Liu, K. Chen, D. Fu, C. Henckel, K. Chaung, S. E. Miranda, S. Dyckman, M. Crum *et al.*, Nat. Commun. **10**, 1 (2019).
[18] A. M. Turing, Phil. Trans. R. Soc. B **237**, 37 (1952).
[19] A. Gierer and H. Meinhardt, Kybernetik **12**, 30 (1972).
[20] J. D. Murray, *Mathematical Biology II: Spatial Models and Biomedical Applications*, Interdisciplinary Applied Mathematics (Springer, New York, 2003).
[21] M. A. Fuentes, M. N. Kuperman, and V. M. Kenkre, Phys. Rev. Lett. **91**, 158104 (2003).
[22] F. Borgogno, P. D'Odorico, F. Laio, and L. Ridolfi, Rev. Geophys. **47** (2009).
[23] R. Martínez-García, J. M. Calabrese, E. Hernández-García, and C. López, Phil. Trans. R. Soc. A **372**, 20140068 (2014).
[24] D. M. Cornforth and K. R. Foster, Nat. Rev. Microbiol. **11**, 285 (2013).
[25] W. H. Burt, J. Mammal. **24**, 346 (1943).
[26] R. Grima, in *Multiscale Modeling of Developmental Systems*, edited by S. Schnell, P. K. Maini, S. A. Newman, and T. J. Newman, Current Topics in Developmental Biology (Academic Press, New York, 2008), Vol. 81, pp. 435–460.
[27] See Supplemental Material at http://link.aps.org/supplemental/10.1103/PhysRevLett.130.058401 for detailed calculations and further discussions, which includes Refs. [19,28–31].
[28] C. Tsallis and D. J. Bukman, Phys. Rev. E **54**, R2197 (1996).
[29] P. V. Paulau, D. Gomila, C. López, and E. Hernández-García, Phys. Rev. E **89**, 032724 (2014).
[30] C. Fernandez-Oto, O. Tzuk, and E. Meron, Phys. Rev. Lett. **122**, 048101 (2019).
[31] D. Ruiz-Reynés, F. Schönsberg, E. Hernández-García, and D. Gomila, Phys. Rev. Res. **2**, 023402 (2020).
[32] S. Pigolotti, C. López, and E. Hernández-García, Phys. Rev. Lett. **98**, 258101 (2007).
[33] R. Martínez-García, J. M. Calabrese, E. Hernández-García, and C. López, Geophys. Res. Lett. **40**, 6143 (2013).
[34] J. D. Murray, *Mathematical Biology: I. An Introduction*, Interdisciplinary Applied Mathematics (Springer, New York, 2002).
[35] J. Hommel, E. Coltman, and H. Class, Transp. Porous Media **124**, 589 (2018).
[36] P. Turchin, *Quantitative Analysis of Movement: Measuring and Modeling Population Redistribution in Animals and Plants* (Sinauer Associates, Sunderland, MA, 1998).
[37] M. E. Cates, D. Marenduzzo, I. Pagonabarraga, and J. Tailleur, Proc. Natl. Acad. Sci. U.S.A. **107**, 11715 (2010).
[38] A. Okubo and S. A. Levin, *Diffusion and Ecological Problems: Modern Perspectives* (Springer Science & Business Media, New York, 2013), Vol. 14.
[39] F. Courchamp, T. Clutton-Brock, and B. Grenfell, Trends Ecol. Evol. **14**, 405 (1999).
[40] E. Colombo and C. Anteneodo, J. Theor. Biol. **446**, 11 (2018).
[41] E. Hernández-García and C. López, Phys. Rev. E **70**, 016216 (2004).
[42] M. Fuentes, M. Kuperman, and V. Kenkre, J. Phys. Chem. B **108**, 10505 (2004).
[43] G. Andreguetto Maciel and R. Martinez-Garcia, J. Theor. Biol. **530**, 110872 (2021).
[44] J. O'Byrne and J. Tailleur, Phys. Rev. Lett. **125**, 208003 (2020).
[45] A. Swain, T. Hoffman, K. Leyba, and W. F. Fagan, Front. Ecol. Evol. **9**, 698041 (2021).
[46] R. B. A. Zinati, C. Duclut, S. Mahdisoltani, A. Gambassi, and R. Golestanian, Europhys. Lett. **136**, 50003 (2022).
[47] R. Grima, Phys. Rev. Lett. **95**, 128103 (2005).
[48] R. Eftimie, G. de Vries, and M. A. Lewis, Proc. Natl. Acad. Sci. U.S.A. **104**, 6974 (2007).
[49] D. Karig, K. M. Martini, T. Lu, N. A. DeLateur, N. Goldenfeld, and R. Weiss, Proc. Natl. Acad. Sci. U.S.A. **115**, 6572 (2018).
[50] J. Liu, R. Martinez-Corral, A. Prindle, D.-Y. D. Lee, J. Larkin, M. Gabalda-Sagarra, J. Garcia-Ojalvo, and G. M. Süel, Science **356**, 638 (2017).
[51] J. G. Orlandi, J. Soriano, E. Alvarez-Lacalle, S. Teller, and J. Casademunt, Nat. Phys. **9**, 582 (2013).

Correction: A sign error has been fixed in an inline equation in the last sentence after Eq. (8).